GRAIN ANGLE EFFECTS ON ACOUSTIC EMISSION (AE) CHARACTERISTICS OF SOUTHERN YELLOW PINE (SYP) COLUMNS UNDER COMPRESSION

Rajan Adhikari

Product Engineer
Weyerhaeuser Technology Center,
Federal Way, WA 98001
E-mail: rajan.adhikari@weyerhaeuser.com

Samuel O. Ayanleye

Staff Engineer
APA – The Engineered Wood Association,
Tacoma, WA 98466
E-mail: samuel.ayanleye@apawood.org

*Edward D. Entsminger†**

Extension Associate III
Department of Wildlife, Fisheries and Aquaculture (WFA),
College of Forest Resources (CFR),
Mississippi State University (MSU) Extension,
Mississippi State, MS 39762-9690
E-mail: edward.entsminger@msstate.edu

Franklin Quin†

Assistant Professor
Department of Sustainable Bioproducts (DSB),
Forest and Wildlife Research Center (FWRC),
College of Forest Resources (CFR),
Mississippi State University (MSU),
Mississippi State, MS 39762-9820
E-mail: fq3@msstate.edu

Wengang Hu

Associate Professor
Nanjing Forestry University (NJFU),
Co-Innovation Center of Efficient Processing and Utilization of Forest Resources,
Nanjing, Jiangsu 210037, People's Republic of China
E-mail: hwg@njfu.edu.cn

*Jilei Zhang**

Warren S. Thompson Professor of Wood Science and Technology,
Department of Sustainable Bioproducts (DSB),
Forest and Wildlife Research Center (FWRC),
College of Forest Resources (CFR),
Mississippi State University (MSU),
Mississippi State, MS 39762-9820
E-mail: jz27@msstate.edu

(Received May 1, 2024)

* Corresponding author
† SWST member

Wood and Fiber Science, 56(4), 2024, pp. 207-221
https://doi.org/10.22382/wfs-2024-19

Abstract. This study investigated the influence of wood grain angle (0°, 10°, 20°, 30°, 45°, 60°, 75°, and 90°) on acoustic emission (AE) characteristics of southern yellow pine columns subjected to compressive loading. Four AE parameters considered were counts, cumulative counts, count rate, and amplitude. The main conclusion was that AE cumulative counts vs time curves can be characterized by three distinct stages in terms of AE count rates: initiation, growth, and acceleration. The initiation stage had a constant mean count rate of 0.33 counts/s compared with the growth stage mean count rate of 19.10 counts/s, whereas the acceleration stage had a mean count rate of 608.40 counts/s. Within each stage, count rates increased as the grain angle increased from 0° to 30°, then dropped as the grain angle further increased to 90°. Maximum AE counts and total cumulative AE counts all increased as the grain angle increased from 0° to 30° and decreased as the grain angle further increased to 90°. Higher AE amplitudes were observed in the yield and failing stages of tested wood columns according to their stress–strain curves plotted together with their corresponding amplitude–time curves. Maximum amplitude increased as the grain angle increased from 0° to 20°, then had a decreasing trend as the grain angle increased to 45°, followed by an increasing trend as the grain angle increased to 75°. These differences in AE characteristics suggested that AE "signatures" in terms of AE signals do exist for timber materials when subjected to compressive loading.

Keywords: Grain angle, acoustic emission (AE), southern yellow pine (SYP), compression, stress–strain.

INTRODUCTION

Wood, a natural renewable resource, is a valuable construction material, because of its low energy consumption, workability, high strength properties, and reliability in structural applications (Hindman and Bouldin 2015; Nguyen et al 2017; Ramage et al 2017). Southern yellow pine (*Pinus* spp. L.) (SYP) is a common and widely used group of commercial softwood species in the United States because of its availability, visual appeal, and good strength properties, making it suitable for use in structural applications (Southern Forest Products Association (SFPA) 2018). The SYP species group grows throughout the southeastern United States, from Virginia to Texas (Junaid et al 2018).

Wood is an orthotropic material and has unique mechanical properties in its three principal plane directions: longitudinal (L), radial (R), and tangential (T) (Green et al 1999; Reiterer and Stanzl-Tschegg 2001; Kretschmann 2010). In lumber, tension and shear failure are considered brash failures. However, compression failure is regarded as a ductile failure (André et al 2013; André et al 2014) and must be considered in designing a building structure. The design parameters mostly considered are bending and compression perpendicular to the grain when the wood is used as a construction material (Turkot 2019; Carmona-Uzcategui 2020; Carmona-Uzcategui et al 2020; Irby et al 2020a; Turkot et al 2020). However, wood is extremely strong in both compression and tension parallel to the grain (Turkot 2019; Carmona-Uzcategui 2020; Turkot et al 2020; Carmona-Uzcategui et al 2020; Irby et al 2020a).

One of the most important variables affecting compression properties in wood is grain orientation (Green et al 1999; Kretschmann 2010). The orientation of grain relative to the strength of lumber is critical in understanding the mechanical properties of wood (Green et al 1999; Kretschmann 2010; Ingemi and Yu 2019; Turkot 2019; Carmona-Uzcategui 2020; Carmona-Uzcategui et al 2020; Irby et al 2020b; Turkot et al 2020). Therefore, the evaluation of strength properties including compression parallel or perpendicular to the grain becomes important for structural design purposes (Green 2001).

Koch (1972) reported that southern yellow pine loaded in compression parallel-to-the-grain developed a visibly well-defined pattern of buckling failures. On the tangential faces of failed rectangular wood columns, the lines of failure make a grain angle of 45° to 60° to the column, longitudinal axial direction, whereas on the radial faces, the lines are about perpendicular to the axial direction. Gupta and Sinha (2012) evaluated the compressive properties of Douglas-fir (*Pseudotsuga menziesii* (Mirb.) Franco) columns with grain angles of 0°, 10°, 20°, 30°, 40°, 50°, 60°, 70°, 80°, and 90° (similar to our Fig 1) and found

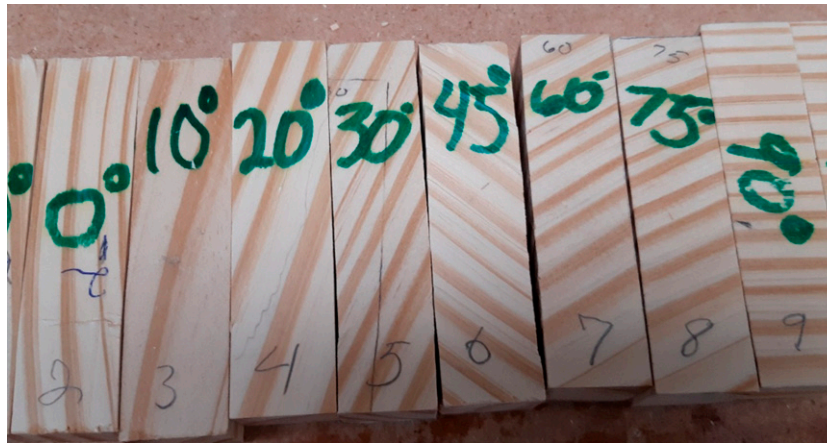

Figure 1. Prepared examples southern yellow pine (*Pinus* spp. L.) wood columns at various cross-grain angles of 0, 10, 20, 30, 45, 60, 75, and 90 degrees, respectively.

that the failure mode changed from shearing parallel to the grain to rolling shear with increasing grain angle orientation. Reiterer and Stanzl-Tschegg (2001) reported that compression failure occurring in columns subjected perpendicular to the grain loading could be attributed to the collapse at the earlywood and latewood sections in the annual rings (the interface section of the wood). Several studies, as reported by Gibson and Ashby (1997) have addressed the complete mechanism responsible for these kinds of failures in softwoods.

Acoustic emission (AE) is defined as the phenomena where transient elastic waves and stresses are generated by the rapid release of energy from a localized source or sources within a material (ASTM 2024). All materials, including wood, contain minute flaws that will initiate microfractures when subjected to stress. These microfractures will enlarge in intermittent step-like bursts as the applied stress increases. During each of these bursts, high-frequency elastic sound waves are produced (Knuffel 1988). These elastic waves released by materials because of fiber breakage, under stress, can be detected and recorded by resonant transducers, such as AE sensors (Sharma 2017; Rescalvo et al 2020). The AE sensing method can allow the detection of destructive changes in materials, like wood, at the moment of being stressed in compression, thereby provide the possibility to follow destructive processes that take place in wood construction beginning with microcracks and ending up in total failure (Reiterer et al 2000; Nasir et al 2022).

The most commonly used parameter for AE signals description is an AE "count." An AE event is "counted" when an AE signal exceeds a preset threshold during any selected portion of the test above any background noises. Derived measurements include the AE cumulative (total) count (Porter et al 1972; Ansell 1982; Sato et al 1984a; Noguchi et al 1992; Raczkowski et al 1999; Ayarkwa et al 2001; Gozdecki and Smardzewski 2005; Ando et al 2006; Chen et al 2006; Ritschel et al 2013) and AE count rate (the number of counts during a given time interval) (Sato et al 1984a; Gozdecki and Smardzewski 2005; Smardzewski and Gozdecki 2007; Du et al 2014). A commonly used frequency domain measurement is the AE amplitude. Hu and Zhang (2022) investigated the peak amplitude of the AE signal. In terms of time-domain vs frequency-domain measurements, AE count rate and cumulative counts are time-domain, whereas the amplitude and peak amplitude are frequency-domain measurements. The time domain refers to analyzing the AE signal as it changes over time, whereas the frequency domain refers to breaking down the AE signal into its constituent frequencies and then analyzing.

Berg and Gradin (2000) investigated the temperature effects on the fracture history of Norway spruce (*Picea abies* (L.) Karst.) under compression in both transverse and longitudinal directions through recording the cumulative AE events. They reported that an ideal temperature level for introducing many failure sites during compression should be well below 120°C and that the longitudinal direction was the most efficient loading direction for introducing flaws in wood during compression (Berg and Gradin 2000). The AE techniques have been effectively used to monitor termite infestation in wood. For instance, AE was used to monitor the activity rhythm and termite feeding of some economically important termites in the United States because microfracturing occurred when wood was attacked by termites that produced AE signals (Mankin et al 2002; Indrayani et al. 2003). The AE techniques have also been used to detect the early stages of wood decay through subjecting wood blocks to compression perpendicular to the grain in the radial (Beall and Wilcox 1987; Raczkowski et al 1999) and tangential directions (Noguchi et al 1992).

However, limited studies have been reported using and assessing AE techniques to monitor the failure progress in wood under a compressive loading (Gong and Smith 2000; Dahlen et al 2018; França et al 2018). Specifically, the AE behavior of SYP wood columns when subjected to external loading with different grain angle orientations has not been fully investigated. The main research investigated the influence of wood grain angles (0°, 10°, 20°, 30°, 45°, 60°, 75°, and 90°) on AE characteristics of SYP columns subjected to compressive loading.

MATERIALS AND METHODS

Materials

One (1) parent SYP (*Pinus* spp. L.) dimensional lumber board with dimensions of 3.810 cm thick × 28.575 cm wide × 3.048 m long was purchased from East Mississippi Lumber Company (Starkville, MS) and planed to a thickness of 2.54 cm.

Experimental Design

A complete one-way factorial experiment with three replicates per experimental combination was conducted to evaluate the effects of grain angle (0°, 10°, 20°, 30°, 45°, 60°, 75°, and 90°), as shown in Fig 1, in reference to the compressive loading direction (that was parallel to the column longitudinal axis). Figure 2 shows a diagram methodology of how each wood column, at various grain angles, was cut from a dimensional lumber board.

AE Apparatus

The AE apparatus consisted of an AE measuring system called Digital Signal Process (μDiSP^{TM}), a laptop computer with Physical Acoustics

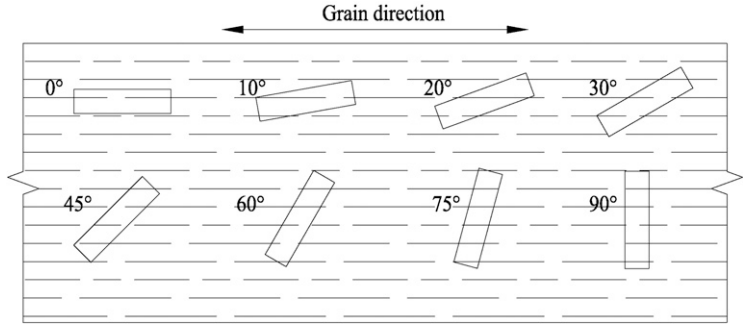

Figure 2. Diagram methodology for cutting wood columns at grain angles of 0°, 10°, 20°, 30°, 45°, 60°, 75°, and 90° from a southern yellow pine (*Pinus* spp. L.) dimensional lumber board.

Corporation (PAC) Acoustic Emission for Windows (AEwin) software installed, and a PAC AE sensor. The AEwin software program collected the AE signal data from the DiSP, recorded it in terms of AE counts and amplitudes vs time, and represented it in a graphical form. The AE sensor operated at a frequency ranging from 50 to 200 kHz. For wood-based materials, the sensor frequency range from 100 to 200 kHz provided sufficient sensitivity to AE emissions of interest (Beall 1985). The AE measuring system had a threshold set to 30 dB, a preamp set to 40 dB, and a filter with the range of 10 to 100 kHz. Gorilla® hot glue sticks (Gorilla Glue Company LLC., Cincinnati, OH) were used in an AdTech® Mini Hi-Temp hot glue gun (Adhesive Technologies, Inc. Hampton, NH) as a couplant between the AE sensor and wood, as the technique to fasten the sensor to the wood sample before testing. The diameter of the AE sensor was 2.71 cm.

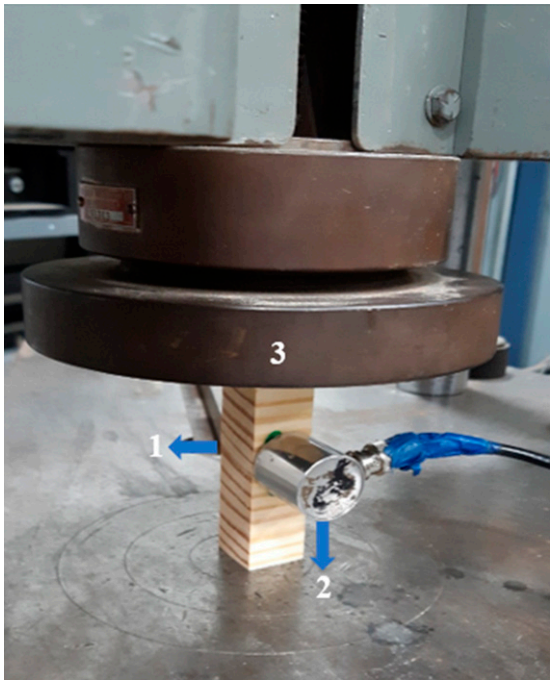

Figure 3. Setup for evaluating acoustic emission (AE) behavior (#2 in image) of southern yellow pine (*Pinus* spp. L.) wood columns (#1 in image) when subjected to a compressive load (#3 in image).

Testing

Twenty-four (24) small clear SYP columns measured 25.40 × 25.40 × 101.60 mm^3 (Fig 1) were cut from the parent board according to American Society for Testing and Materials (ASTM) Standard D143 – 23 (ASTM 2023). Before compression testing, the short columns were conditioned to constant mass in an environmental conditioning chamber for a minimum of three weeks at 22°C and 55.0% RH, and the dimensions were recorded. Figure 3 shows the setup for evaluating AE behavior of SYP wood columns subjected to compressive stress. One AE sensor was hot glued onto the wood column surface at the middle of the column. All columns were mechanically tested on an Instron® Tinius-Olsen Universal Testing Machine at a crosshead speed of 0.30 mm per minute according to the ASTM D143 – 23 standard (ASTM 2023). Load–deformation curves with synchronous AE activities were recorded. Before loading each column at test, physical volume dimensions (width, depth, and length) of each sample were measured using a Mitutoyo Absolute Digital Caliper (Model No. CD-6" CSX, Serial No. 13152425; Kawasaki, Japan, Asia) and recorded. Failure modes for each tested column were evaluated, determined, and recorded. The physical properties such as MC and specific gravity (SG) of the samples were determined by oven-dry mass at 103°C in a Blue M Electric Company Dry Oven (Model B-3005-Q, Blue Island, IL). The coefficient of variation (COV) was determined for all samples.

Statistical Analysis

Data were analyzed using Microsoft Excel 365 software (Microsoft Corporation). SigmaPlot version 14.5 (Inpixon, Palo Alto, CA) software was used for graph plots, scientific graphing, and data analysis.

RESULTS AND DISCUSSION

Physical Properties

The MC values of tested wood columns ranged from 7.70 to 12.80% (oven-dry basis), with an

Table 1. Summary of failure modes recorded for three southern yellow pine (SYP) columns for each of eight different grain angles evaluated under compression.

	Grain angle (°)[a]							
Replicate	0	10	20	30	45	60	75	90
1	B	B	S	S	CO+B	CO+B	CO+B	CO
2	B	B	S	S	CO+B	CO+B	CO+B	CO
3	B	B	S	S	CO+B	CO+B	CO+B	CO

[a]Where B, buckling failure; S, shearing failure; CO, compression failure; and CO+B, compression and buckling failure combination.

average of 10.37% and a COV of 11.43%. The SG values ranged from 0.39 to 0.59, with an average of 0.49 and corresponding COV of 9.61%.

Mechanical Properties

Failure modes. Table 1 summarizes the failure modes recorded for each SYP column evaluated in this study. The columns with 0° and 10° grain angles developed a visibly well-defined pattern of buckling failures. Figure 4 shows the typical failure modes observed in mechanically tested SYP columns. The lines of failure made an angle to the column in a longitudinal direction on the tangential faces of failed columns (Fig 4[a]). The lines were perpendicular to the longitudinal direction on the radial faces and were similar to those described in Koch (1972). This buckling failure was caused mainly by shear failure that occurred at the overlap of the tapered ends of the tracheids, which comprise most of the volume in SYP. This was mainly because under a compressive load parallel to wood cells, the longitudinal direction overlaps the tapered ends of the tracheids as they must induce shear forces between adjacent cells (Koch 1972). Columns with 20° and 30° grain angles all experienced shear parallel to the grain (Fig 4[b]). The grain angles of 20° were observed in shear failure, whereas the 30° was related to the impact of wood density on its mechanical properties, as a change in strength is normally observed within annual rings and at the ring border as described by Jakob et al (1994). The shear failures observed in this study occurred mainly in the earlywood sections of the tested columns because of the collapsing separation of the earlywood regions at the annual growth rings (Reiterer and Stanzl-Tschegg 2001) or wood fiber misalignment (Poulsen et al 1997). Columns with 45° to 75° grain angles failed with earlywood and latewood compression as shown by the "S-wavy" shaped buckling (Fig 4[c]), whereas the 90° samples failed in compression at the earlywood/latewood interface (Fig 4[d]). These compression failures could be attributed to wood tracheid walls bent inward and distorted sideways (Koch 1972) and collapse at the earlywood/latewood interface (Reiterer and Stanzl-Tschegg 2001). In general, the failure modes observed were similar to those observed in other softwood studies (Ayres 1920; Martel 1920; Hankinson 1921; Osgood 1928;

Figure 4. Typical failure modes observed in mechanically tested southern yellow pine (*Pinus* spp. L.) wood columns: (a) buckling (radial face, 0° column); (b) shearing (20° column); (c) compression and "S-wavy shaped" buckling (45° column); and (d) horizontal compression (90° columns).

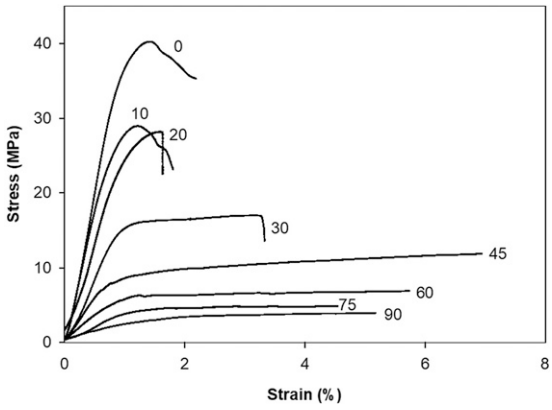

Figure 5. Typical stress–strain curves showing each of the eight-grain angles evaluated on southern yellow pine (SYP) wood columns subjected to compressive loading.

Kojis and Postweilder 1953; Kim 1986; Reiterer and Stanzl-Tschegg 2001).

Stress–strain curves. Typical stress–strain curves of the tested SYP columns are illustrated in Fig 5. These curves indicated that the columns with grain angles between 0° and 20° behaved like brittle materials that had an initial linear stage, a smooth nonlinear curve representing the transition between the proportional limit and ultimate stresses, and then a sharp decrease in stress after reaching the ultimate load (Reiterer and Stanzl-Tschegg 2001; Güntekin and Aydin 2013). Columns with grain angles ranging from 45° to 90° behaved like a ductile or plastic-like material that had poorly deformed ultimate stresses. Columns with a grain angle of 30° behaved like ductile materials with more plastic deformation before failure. The resistance to an external compressive load with grain angles ranging from 0° to 20° decreased sharply after reaching its ultimate value. This could be because of cracking that developed under the compressive stress (Berg and Gradin 2000). These cracks could be related to shear failures of tracheids because of the different separations along the middle lamella, particularly in axial parenchyma cells of certain wood species, but these cells are generally absent in pine. Alternatively, tracheids could separate within the cell wall between the S_1 and S_2 layers (Koch 1972). In the cases of wood columns with grain angles from 45° to 90°, stresses continued increasing with strain beyond their proportional limit; however, at a lower rate of change. Compaction of the wood occurred with increasing deformation after the flattening and failure of the cell walls. This was followed by a continuous rise in the resistance of the compressed columns. Stress at the proportional limit was used to determine allowable stresses in compression perpendicular to the grain because ultimate stresses for this property were not clearly defined (FPL 2021). This recommendation would also be extended for columns with grain angles greater than 30°. Figure 6 plots experimental means of ultimate compressive strength (Fig 6[a]) and stiffness (Fig 6[b]) of the SYP columns together with their corresponding estimated values using Hankinson's formula (FPL 2021) (see Eq 1)

$$N = \frac{\mathrm{PQ}}{P\sin^n\theta + Q\cos^n\theta} \tag{1}$$

where N can be the modulus of elasticity as well as strength properties at angle θ from the fiber direction, Q is the strength perpendicular to the grain, P is the strength parallel to the grain, and n is an empirically determined constant. The calculated ratios (Q/P) based on the experimental mechanical properties were 0.08 (3.28/41.94) and 0.09 (0.37/3.90) for strength and stiffness, respectively. This was close to 0.10, therefore, the empirically determined constant, $n = 2.50$ was considered in Hankinson's formulas for calculating both properties (FPL 2021). Figure 6 indicated that reasonably accurate estimates were obtained using Hankinson's formula for both compression strength and stiffness of SYP wood columns evaluated in this study. The substantial drop in compressive strength starting at the 20° grain angle was attributed to wood fiber misalignment and shearing (Poulsen et al 1997). Reiterer and Stanzl-Tschegg (2001) and Güntekin and Aydin (2013) also indicated that irreversible shear deformation occurred at annual ring borders of softwood species subjected to compressive loads parallel to the grain, causing a steep decrease in strength.

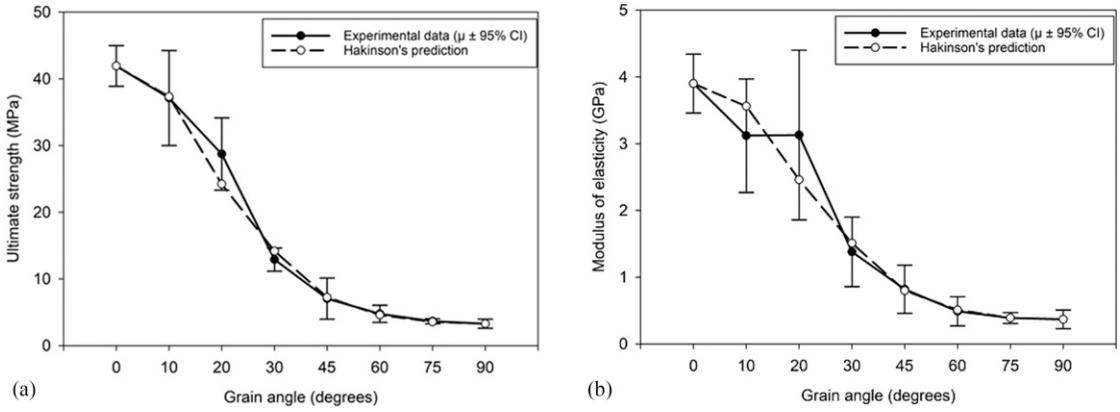

Figure 6. Experimental mean ultimate compressive strength (a) and stiffness (b) values of mechanically tested southern yellow pine (SYP) wood columns at eight different grain angles plotted with their corresponding approximated values using Hankinson's formula.

Cumulative AE Counts–Time Curves

Figure 7 shows a typical cumulative AE counts-time curve plotted with the corresponding stress–strain curve, indicating the damage progression observed in the SYP columns. Three distinct stages were identified in terms of changes in slope (ie, AE cumulative counts) of the cumulative AE counts–time curve: initiation, growth, and acceleration (Raczkowski et al 1994; Du et al 2014). The initiation stage (0 – ~50-100 s) was the first linear portion where the AE count rate was slower (Beall and Wilcox 1987) and constant

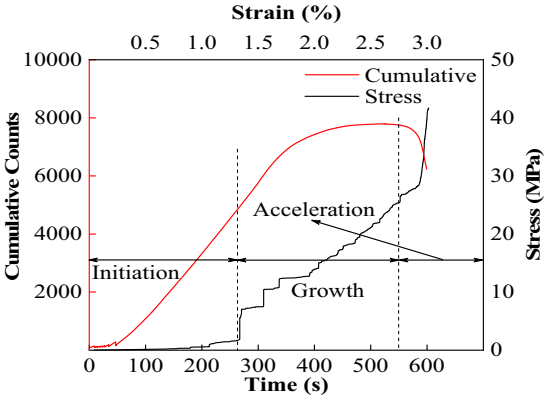

Figure 7. A typical cumulative counts-time curve recorded together with its corresponding stress–strain curve representing acoustic emission (AE) behavior of southern yellow pine (SYP) wood columns subjected to compressive loading.

(Figure 7). Fewer counts were recorded in the initiation stages because microcracks within wood cell walls can occur at stress levels well below the proportional limit (Bodig and Jayne 1982). These microcracks can be detected using AE sensing devices (DeBaise et al 1966) even though these cracks generally do not continue to grow if the load is cyclical, in accordance with the Kaiser Effect (Beall and Wilcox 1987). The growth stage in the second curve portion (~100-300 s) showed a much higher AE count rate relative to the initiation stage (Raczkowski et al 1994) because more cracks developed and propagated as the applied load increased (Bodig and Jayne 1982). Therefore, the growth stage can be considered as a transitional progressive region between the initiation and acceleration stages where the AE count rate changed from relatively low (0.33 counts/s) to higher (608.40 counts/s). The acceleration stage was the third portion (>300 s) where the AE count rate transitioned to an exponential high and constantly increased (Raczkowski et al 1994) because of the collective increase in crack growth. This accelerated crack growth can decrease resistance to stresses and generated more AE activity than the growth stage.

A linear regression method was used to approximate the slope of each of the three stages for each individual AE cumulative counts-time curve for all tested columns. Calculated slope values of all

Table 2. Summary of acoustic emission (AE) count rate values (counts/s) for each of three stages of AE cumulative counts–time curves recorded for mechanically testing southern yellow pine (SYP) columns under compression.

Stages	Mean (counts/s)	Coefficient of variation (COV) (%)	Range (counts/s)
Initiation	0.33	100.0	0.01-1.17
Growth	19.10	149.0	1.07-106.00
Acceleration	608.40	127.0	7.00-2240.00

tested columns at each stage were pooled together. Table 2 summarizes the mean values of the calculated AE count rates together with their corresponding COV values and ranges for each of the three stages. The mean AE count rates were 0.33, 19.10, and 608.40 counts/s for the initiation, growth, and acceleration stages, respectively, indicating that the AE count rate in the initiation stage was much lower than in the growth stage, whereas the count rate in the acceleration stage was much higher than in the growth stage. In addition, larger COV values of count rates ranging from 100.0 to 149.0% were observed in the three stages.

Figure 8 shows mean AE count rates vs grain angle within each stage in AE cumulative counts–time curves of all tested SYP columns. The AE count rate generally increased as the grain angle increased from 0° to 30°, then decreased as the grain angle further increased. The minor changes in the AE count rate within each stage become less important because the differences in magnitude between stages were so large.

Figure 9 plots typical AE counts–time curves of the SYP columns evaluated in this study and shows that some patterns could be identified. There was one peak for columns with grain angles ranging from 0° to 20° (Fig 9[a]–[c]) during the failure process after the stress passed its ultimate value as these columns lost the ability to resist compression loading. This might suggest that the one-peak pattern could be generated by sheared wood cell (like tracheids) walls in compressed SYP columns (Table 1). As the grain angle increased to 30°, the one-peak pattern was still observed in one of the three tested columns (Fig 9[d]), but the other two columns exhibited a different pattern in which two peaks appeared near the point where the stress just exceeded the proportional limit, in addition to the one peak occurring at their failing region (Fig 9[e]). As grain angles further increased above 45°, this pattern of more peaks appearing after the proportional limit (in the yield region) became more common (Fig 9[f] and [g]). The pattern then became one-peak in the yield region right as the stress passed the proportional limit (Fig 9[h] and [i]). The AE count peak patterns observed in SYP columns with grain angles ranging from 45° to 75° suggested that the one-peak pattern could be generated by tracheid wall bending and earlywood and latewood cell wall collapse or flattening. This might suggest that one-peak in counts–time curves could signal the beginning of the cell wall flattening process.

In summary, these different AE patterns that featured count peaks observed in tested SYP columns with different grain angles suggested the existence of some "signatures" in terms of AE signals, and these "signatures" could be related to the different wood fibers or cell failure modes and

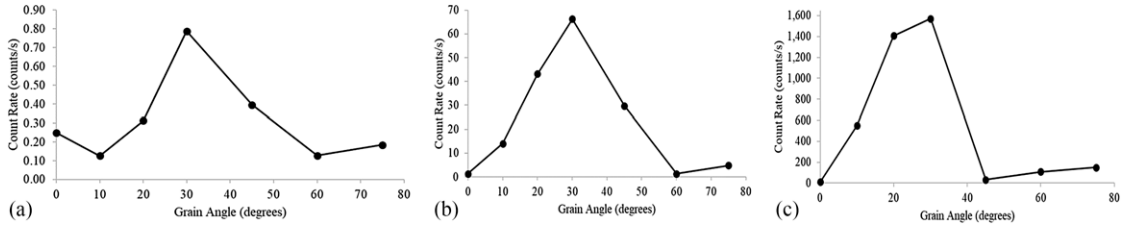

Figure 8. Mean acoustic emission (AE) count rate vs grain angle curves plotted for three stages: (a) initiation, (b) growth, and (c) acceleration as identified in the cumulative AE counts–time curves for the southern yellow pine (SYP) wood columns.

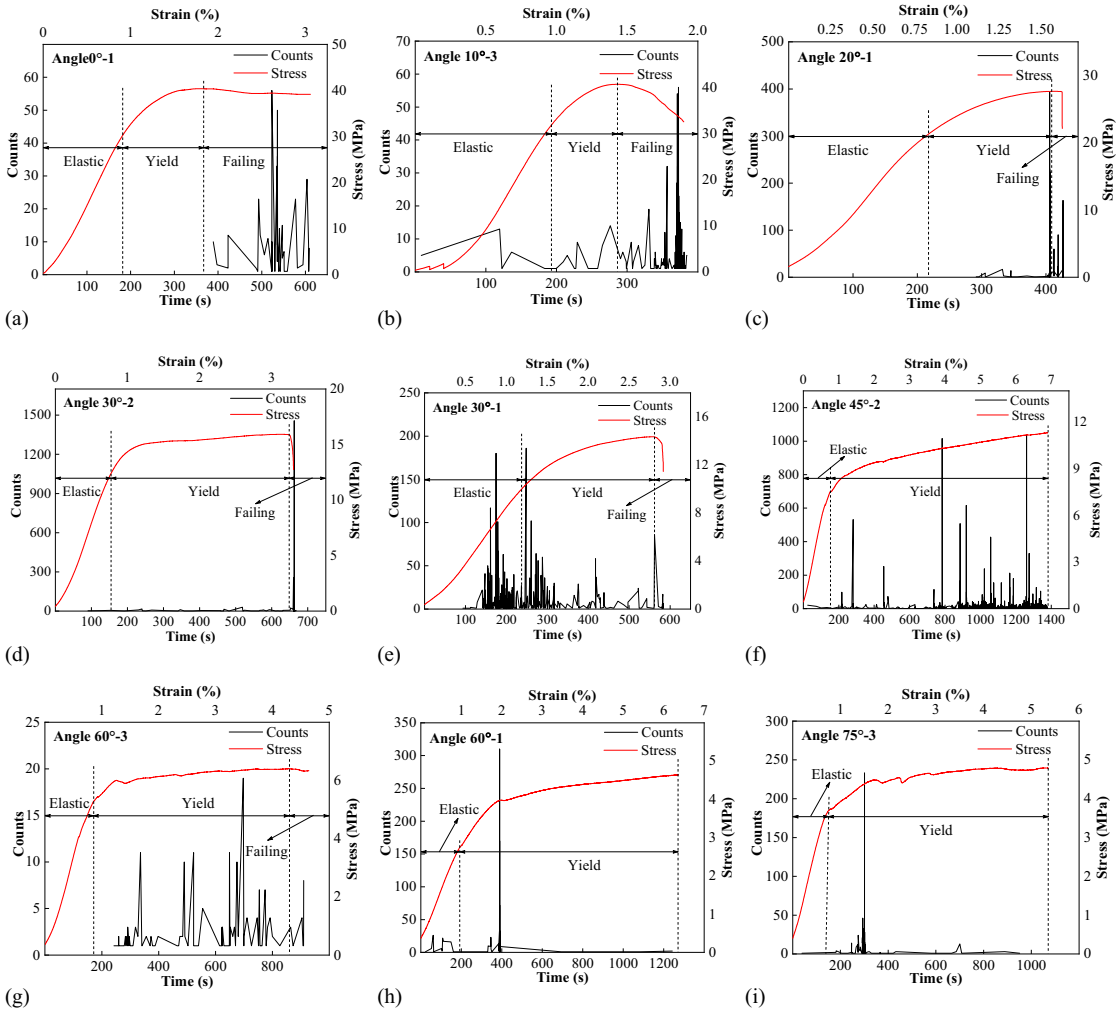

Figure 9. Typical counts–time curves plotted together with their corresponding stress–strain curves for tested southern yellow pine (SYP) wood columns with grain angles: 0° (a), 10° (b), 20° (c), 30° (d), 30° (e), 45° (f), 60° (g), 60° (h), and 75° (i), representing acoustic emission (AE) behavior of these columns in terms of different peak patterns.

processes when subjected to compressive stresses. These "signatures" could be used for nondestructive evaluation (NDE) of wood structures. Table 3 summarizes and Fig 10 plots the mean values of maximum AE counts (Fig 10[a]) and total cumulative AE count emissions (Fig 10[b]) of tested SYP columns, and these values vs grain angle. Maximum AE counts had large COV's ranging from 17.0 to 162.0%, whereas the total cumulative AE counts COV values ranged from 31.0 to 170.0%. The general trend was that as the grain angle increased from 0° to 30°, maximum AE counts and total cumulative AE counts all increased, then decreased as the grain angle further increased from 30° to 90°. Less than 36 counts were recorded for the SYP columns with a 90° grain angle. Fewer AE events recorded in this study could be because of micro cracking produced by cell wall deformation and flattening that generated fewer AEs or lower dB signals.

Table 3. Mean values of maximum acoustic emission (AE) counts and total cumulative counts of mechanically tested southern yellow pine (SYP) columns with different grain angles.[a]

Angle (°)	Maximum counts	Total cumulative counts
0	37 (17)	266 (59)
10	329 (111)	3303 (61)
20	3112 (104)	6092 (31)
30	4299 (141)	12,646 (123)
45	360 (162)	6929 (170)
60	208 (79)	693 (59)
75	779 (117)	6897 (145)
90	30 (119)	36 (125)

[a]Values represent means of three replicates per treatment. The numbers within parentheses indicate the coefficient of variation (COV).

This suggests that an adjustment reducing the threshold setting or increasing the preamp value might be needed for future studies.

AE Amplitude

Figure 11 shows typical AE amplitude–time curves plotted together with the corresponding stress–strain curves for the SYP columns tested in this study. In general, the AE signals with higher AE amplitudes were observed in the yield and failing stages (Fig 11[a]–[d]) and yield stages (Fig 11[e]–[g]). These values ranged from 60 to 100 dB. The mean values of maximum AE peak amplitude are summarized in Table 4 and plotted

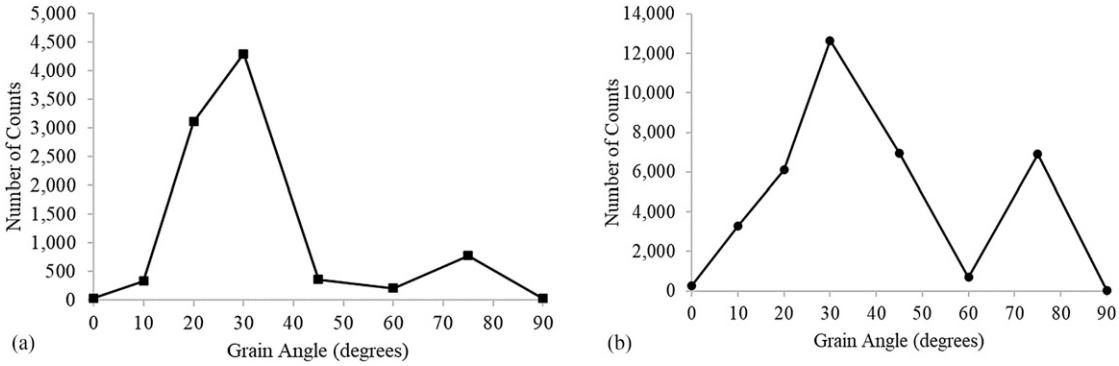

Figure 10. Mean values of maximum acoustic emission (AE) counts (a) and total cumulative acoustic emission counts (b) as a function of grain angle of mechanically tested southern yellow pine (SYP) wood columns in this study.

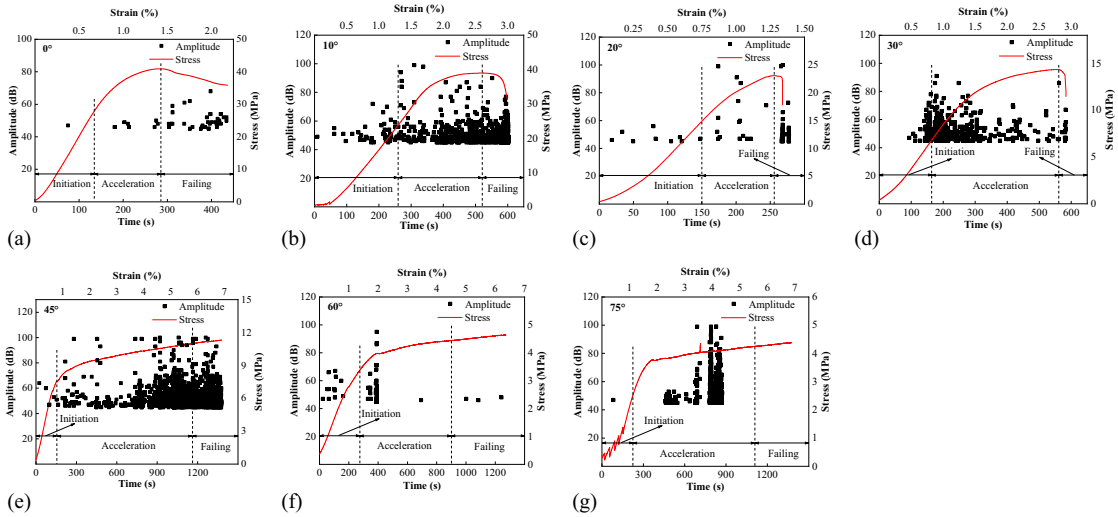

Figure 11. Typical acoustic emission (AE) amplitude vs time curves plotted together with their corresponding stress–strain curves for southern yellow pine (SYP) columns mechanically tested at grain angles of: (a) 0°, (b) 10°, (c) 20°, (d) 30°, (e) 45°, (f) 60°, and (g) 75°.

Table 4. Mean values of maximum acoustic emission (AE) amplitude (dB) on southern yellow pine (SYP) columns that were mechanically tested at the indicated grain angles.[a]

Grain angle (°)						
0	10	20	30	45	60	75
69.3 (12)	89.7 (15)	99.7 (1)	96.7 (5)	76.7 (28)	84.7 (25)	94.0 (8)

[a]Values represent means of three replicates per treatment. The numbers within parentheses indicate the coefficient of variation (COV).

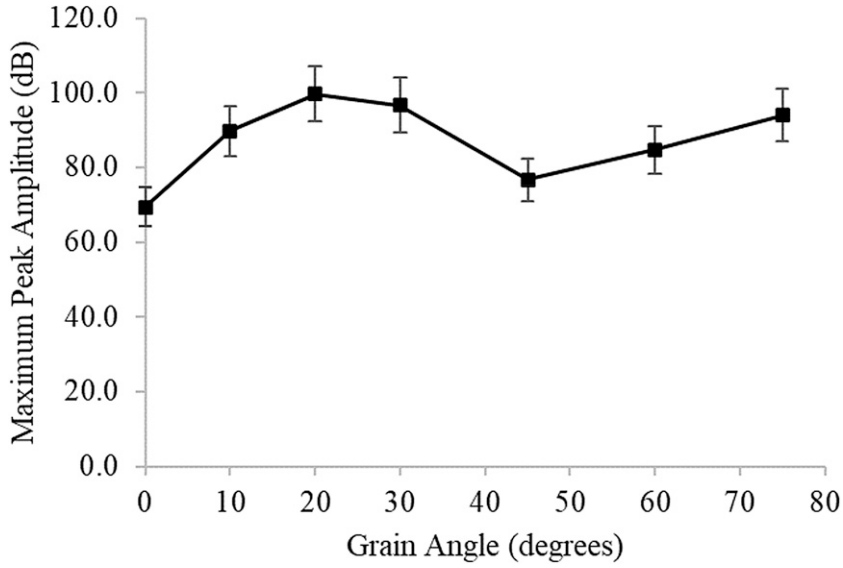

Figure 12. Mean values of maximum acoustic emission (AE) peak amplitude with standard error (SE) bars of the mean vs grain angle plot for southern yellow pine (SYP) wood columns assessed in this study.

in Fig 12. These results indicated that the maximum amplitude increased as the grain angle increased from 0° to 20° grain angles, then decreased as the grain angle decreased to 45°, followed by an increasing trend as the grain angle increased further to 75°. This pattern could be related to different micro-cracking failures occurring in SYP columns as the grain angle changed from 0 to 75°. In particular, the transition point of the failure mode of cells can be identified at 45°, where there was a change from shearing to bending and flattening.

CONCLUSIONS

1. Three distinct stages were identified in the cumulative AE counts–time curve in terms of AE count rate which included initiation, growth, and acceleration. The lowest count rate was observed at the initiation stage (0.33 counts/s) whereas the highest rate was observed at the acceleration stage (608.40 counts/s).
2. The AE count rate increased as the grain angle increased from 0° to 30° and then decreased as the grain angle further increased beyond 30°. We observed the same trend for maximum AE counts and total cumulative AE counts.
3. The maximum AE amplitude increased as the grain angle increased from 0° to 20°, then began a decreasing trend as the grain angle decreased to 45°, followed by an increasing trend as the grain angle increased to 75°. The AE signals with a higher

amplitude were observed in the yield and failing stages.

4. Some "signatures" in terms of AE signals do exist and could be related to different responses in wood fibers or cell failure modes such as shearing, bending, and compression and their corresponding development processes.
5. The combination of these "signatures" could be used to develop an NDE device algorithm to detect the progression of mechanical damage in structures constructed using SYP columns.

ACKNOWLEDGMENTS

The authors acknowledge Mississippi State University (MSU), College of Forest Resources (CFR), Department of Sustainable Bioproducts (DSB), and the Forest and Wildlife Research Center (FWRC) for providing financial support for this novel research. This publication is a contribution of the Forest and Wildlife Research Center (FWRC) at Mississippi State University (MSU).

REFERENCES

Ando K, Hirashima Y, Sugihara M, Hirao S, Sasaki Y (2006) Microscopic processes of shearing fracture of old wood, examined using the acoustic emission technique. J Wood Sci 52(6):483-489. https://doi.org/10.1007/s10086-005-0795-7.

André A, Kliger R, Asp LE (2014) Compression failure mechanism in small-scale timber specimens. Constr Build Mater 50(15 January 2014):130-139. https://doi.org/10.1016/j.conbuildmat.2013.09.018.

André A, Kliger R, Olsson R (2013) Compression failure mechanism in small-scale wood specimens reinforced with CFRP: An experimental study. Constr Build Mater 41(April 2013):790-800. https://doi.org/10.1016/j.conbuildmat.2012.12.038.

Ansell MP (1982) Acoustic emission from softwood in tension. Wood Sci Technol 16(1):35-57. https://doi.org/10.1007/BF00351373.

ASTM (2023) D 143-23. Standard test methods for small clear specimens of timber. American Society for Testing and Materials, West Conshohocken PA. https://www.astm.org/d0143-23.html.

ASTM (2024) E 1316-24b Standard terminology for nondestructive examinations. American Society for Testing and Materials, West Conshohocken, PA. https://www.astm.org/e1316-24.html.

Ayarkwa J, Hirashima Y, Ando K, Sasaki Y (2001) Monitoring acoustic emission to predict modulus of rupture of finger-joints from tropical African hardwoods. Wood Fiber Sci 33(3):450-464. https://wfs.swst.org/index.php/wfs/article/view/130/130.

Ayres QC (1920) Crushing strength of southern pine at angles to grain. Eng News-Record 85(14):653-654. https://archive.org/details/engineeringnewsr85newy/page/653/mode/1up. (30 August 2024).

Beall FC (1985) Relationship of acoustic emission to internal bond strength of wood-based composite panel materials. J Acoustic Emission 4(1):19-29. http://www.aewg.org/jae/JAE-Vol_04-1985.pdf. (30 August 2024).

Beall FC, Wilcox WW (1987) Relationship of acoustic emission during radial compression to mass loss from decay. Forest Prod J 37(4):38-42. http://kb.forestprod.org/Main/ind/?id=66433.

Berg JE, Gradin PA (2000) Effect of temperature on fracture of spruce in compression, investigated by use of acoustic emission monitoring. J Pulp Paper Sci 26(8):294-299. https://www.researchgate.net/publication/274256796_Effect_of_Temperature_on_Fracture_of_Spruce_in_Compression_Investigated_by_Use_of_Acoustic_Emission_Monitoring. (30 August 2024).

Bodig J, Jayne BA, (1982) Mechanics of wood and wood composites. Van Nostrand Reinhold Company Inc., New York. 712 pp. ISBN-10: 0442008228. https://archive.org/details/mechanicsofwoodw0000bodi/page/n5/mode/2up. (30 August 2024).

Carmona-Uzcategui MG (2020) Properties of four domestic hardwood species. MS thesis, Mississippi State, MS: Mississippi State University. 54 pp. https://scholarsjunction.msstate.edu/td/3662. (30 August 2024).

Carmona-Uzcategui MG, Seale RD, França FJN (2020) Physical and mechanical properties of clear wood from red oak and white oak. BioRes 15(3):4960-4971. https://bioresources.cnr.ncsu.edu/resources/physical-and-mechanical-properties-of-clear-wood-from-red-oak-and-white-oak/.

Chen Z, Gabbitas B, Hunt D (2006) Monitoring the fracture of wood in torsion using acoustic emission. J Mater Sci 41(12):3645-3655. https://doi.org/10.1007/s10853-006-6292-6.

Dahlen J, Auty D, Eberhardt TL (2018) Models for predicting specific gravity and ring width for loblolly pine from intensively managed plantations, and implications for wood utilization. Forests 9(6):292-312. https://doi.org/10.3390/f9060292.

DeBaise G, Porter A, Pentoney R (1966) Morphology and mechanics of wood fracture. Mat Res Stand 6(10):493-499. https://www.cabidigitallibrary.org/doi/full/10.5555/19660602840. (30 August 2024).

Du Y, Zhang J, Shi S (2014) Acoustic emission of bolt-bearing testing on structural composite lumbers. Wood Fiber Sci 46(1):118-126. https://wfs.swst.org/index.php/wfs/article/view/637.

FPL (2021) Wood handbook: Wood as an engineering material. Gen Tech Rep FPL-GTR-282. USDA For

Serv Forest Products Laboratory, Madison, WI. 546 pp. https://www.fpl.fs.usda.gov/documnts/fplgtr/fplgtr282/fpl_gtr282.pdf. (30 August 2024).

França TSA, França FJN, Seale RD, Shmulsky R (2018) Bending strength and stiffness of No. 2 grade southern pine lumber. W&Fs 50(2):205-219. https://wfs.swst.org/index.php/wfs/article/view/2698.

Gibson LJ, Ashby MF, (1997) Cellular solids: Structure and properties, 2nd edition. Cambridge University Press, Cambridge, England, United Kingdom. 510 pp. ISBN: 9781139878326. https://doi.org/10.1017/CBO9781139878326.

Gong M, Smith I (2000) Failure of softwood under static compression parallel to grain. J Institute Wood Sci 15(4): 204-210. https://www.researchgate.net/publication/287178221_Failure_of_softwood_under_static_compression_parallel_to_grain. (30 August 2024).

Gozdecki C, Smardzewski J (2005) Detection of failures of adhesively bonded joints using the acoustic emission method. Holzfor 59(2):219-229. https://doi.org/10.1515/HF.2005.035.

Green DW, (2001) Wood: Strength and stiffness. Pages 9732-9736 *in* KH Jürgen Buschow, RW Cahn, MC Flemings, B Ilschner, EJ Kramer, S Mahajan, and P Veyssière, eds. Encyclopedia of materials: Science and technology, 2nd edition. Elsevier, Amsterdam and New York. ISBN: 9780080431529. https://doi.org/10.1016/B0-08-043152-6/01766-6.

Green DW, Winandy JE, Kretschmann DE (1999) Chapter 4: Mechanical properties of wood. Pages 4-1 to 4-45 in Wood handbook: Wood as an engineering material. Gen Tech Rep FPL-GTR-113. USDA For Serv Forest Products Laboratory, Madison, WI. 463 pp. https://doi.org/10.2737/FPL-GTR-113.

Güntekin E, Aydin TY (2013) Effects of moisture content on some mechanical properties of Turkish red pine (*Pinus brutia* Ten.). Pages 878-883 *in* Proceedings, International Caucasia Forestry Symposium, 24-26 October 2013, Artvin, Turkey. https://www.researchgate.net/publication/281236918_Effects_of_Moisture_Content_on_Some_Mechanical_Properties_of_Turkish_Red_Pine_Pinus_brutia_Ten. (30 August 2024).

Gupta R, Sinha A (2012) Effect of grain angle on shear strength of Douglas-fir wood. Holzforschung 66(5):655-658. https://doi.org/10.1515/hf-2011-0031.

Hankinson RL (1921) Investigation of crushing strength of spruce at varying angles of grain. United States Army, Engineering Division, Washington D.C. McCook Field Report, Serial No. 1570. Air Service Information Circular No. 259, Volume 3, 16 pp. https://content.lib.auburn.edu/digital/collection/asic/id/382/rec/18. (30 August 2024).

Hindman DP, Bouldin JC (2015) Mechanical properties of southern pine cross-laminated timber. J Mater Civ Eng 27(9):04014251. https://doi.org/10.1061/(ASCE)MT.1943-5533.0001203.

Hu W, Zhang J (2022) Effect of growth rings on acoustic emission characteristic signals of southern yellow pine wood cracked in mode I. Constr Build Mater 329(25 April 2022):127092. https://doi.org/10.1016/j.conbuildmat.2022.127092.

Indrayani Y, Nakayama T, Yanase Y, Fujii Y, Yoshimura T, Imamura Y (2003) Feeding activities of the drywood termite *Cryptotermes domesticus* (Haviland) under various relative humidity and temperature conditions using acoustic emission monitoring. Jpn J Environ Entomol Zoo 14(4):205-212. https://www.jstage.jst.go.jp/article/jjeez/14/4/14_205/_pdf. (30 August 2024).

Ingemi CM, Yu T (2019) Detection of grain angle in wood specimens using synthetic aperture radar imaging. Proceedings, Society of Photo-Optical Instrumentation Engineers (SPIE), Volume 10971, Nondestructive Characterization and Monitoring of Advanced Materials, Aerospace, Civil Infrastructure, and Transportation XIII, 109710U. SPIE Smart Structures and Nondestructive Evaluation Conference, April 1, 2019, Denver, Colorado. https://doi.org/10.1117/12.2513972.

Irby NE, França FJN, Barnes HM, Seale RD, Shmulsky R (2020a) Effect of growth rings per inch and density on compression parallel to grain in southern pine lumber. BioRes 15(2):2310-2325. https://bioresources.cnr.ncsu.edu/resources/effect-of-growth-rings-per-inch-and-density-on-compression-parallel-to-grain-in-southern-pine-lumber/.

Irby NE, França FJN, Barnes HM, Seale RD, Shmulsky R (2020b) Effect of growth rings per inch and specific gravity on compression perpendicular to grain in No. 2: 2 by 8 and 2 by 10 southern pine lumber. For Prod J 70(2):213-220. https://doi.org/10.13073/FPJ-D-19-00043.

Jakob HF, Fratzl P, Tschegg SE (1994) Size and arrangement of elementary cellulose fibrils in wood cells: A small-angle X-ray scattering study of *Picea abies*. J Struct Biol 113(1):13-22. https://doi.org/10.1006/jsbi.1994.1028.

Junaid O, Owens FC, Entsminger ED, Seale RD, Shmulsky R (2018) Strength and stiffness properties of small clear specimens taken from commercially procured No. 2 2×8 and 2×10 southern pine dimension lumber. Wood Fiber Sci 50(3):363-369. https://wfs.swst.org/index.php/wfs/article/view/2732.

Kim KY (1986) A note on the Hankinson formula. Wood Fiber Sci 18(2):345-348. https://wfs.swst.org/index.php/wfs/article/view/698.

Knuffel WE (1988) Acoustic emission as strength predictor in structural timber. Holzfor 42(3):195-198. https://doi.org/10.1515/hfsg.1988.42.3.195.

Koch P, (1972) Utilization of the southern pines. Agriculture Handbook No. 420. Volume 1 – The raw material. USDA U.S. Forest Service, Southern Forest Experiment Station. https://www.srs.fs.usda.gov/pubs/ah/ah420_vol1.pdf. (30 August 2024).

Kojis DD, Postweilder RS (1953) Allowable loads for common bolts at various angles to the grain for southern yellow pine. For Prod J 3(3):21-26. http://kb.forestprod.org/Main/ind/?id=70289.

Kretschmann DE (2010) Chapter 5: Mechanical properties of wood. Pages 5-1 to 5-44 *in* Wood handbook – Wood as an engineering material. Gen Tech Rep FPL-GTR-190. USDA For Serv Forest Products Laboratory, Madison, WI. 509 pp. https://doi.org/10.2737/FPL-GTR-190.

Mankin RW, Osbrink WL, Oi FM, Anderson JB (2002) Acoustic detection of termite infestations in urban trees. J Econ Entomol 95(5):981-988. https://doi.org/10.1093/jee/95.5.981.

Martel RR (1920) Tests of bearing strength of redwood agree with Howe's Formula. Eng News-Record 85(20): 959. https://archive.org/details/engineeringnewsr85newy/page/958/mode/2up. (30 August 2024).

Nasir V, Ayanleye S, Kazemirad S, Sassani F, Adamopoulos S (2022) Acoustic emission monitoring of wood materials and timber structures: A critical review. Constr Build Mater 350(3 October 2022):128877. https://doi.org/10.1016/j.conbuildmat.2022.128877.

Nguyen TT, Ji X, Van Nguyen TH, Guo M (2017) Wettability modification of heat-treated wood (HTW) via cold atmospheric-pressure nitrogen plasma jet (APPJ). Holzfor 72(1):37-43. https://doi.org/10.1515/hf-2017-0004.

Noguchi M, Ishii R, Fujii Y, Imamura Y (1992) Acoustic emission monitoring during partial compression to detect early stages of decay. Wood Scitechnol 26(4): 279-287. https://doi.org/10.1007/BF00200163.

Osgood WR (1928) Compressive stress on wood surfaces inclined to the grain. Eng News-Record 100(6):243-244. https://archive.org/details/sim_enr_1928-02-09_100_6/page/242/mode/2up. (30 August 2024).

Porter AW, El-Osta ML, Kusec DJ (1972) Prediction of failure of finger joints using acoustic emissions. Forest Prod J 22(9):74-82. http://kb.forestprod.org/Main/ind/?id=70090.

Poulsen JS, Moran PM, Shih CF, Byskov E (1997) Kink band initiation and band broadening in clear wood under compressive loading. Mech Mater 25(1):67-77. https://doi.org/10.1016/S0167-6636(96)00043-9.

Raczkowski J, Lutomski K, Moliński W, Woś R (1999) Detection of early stages of wood decay by acoustic emission technique. Wood Sci Technol 33(5):353-358. https://doi.org/10.1007/s002260050121.

Raczkowski J, Moliński W, Ranachowski Z (1994) Acoustic emission in fracture mechanics of wood. J Theor Appl Mech 32(2):299-322. http://www.ptmts.org.pl/jtam/index.php/jtam/article/viewFile/v32n2p299/1082. (30 August 2024).

Ramage MH, Burridge H, Busse-Wicher M, Fereday G, Reynolds T, Shah DU, Wu G, Yu L, Fleming P, Densley-Tingley D, Allwood J, Dupree P, Linden PF, Scherman O (2017) The wood from the trees: The use of timber in construction. Renew Sust Energ Rev 68(1): 333-359. https://doi.org/10.1016/j.rser.2016.09.107.

Reiterer A, Stanzl-Tschegg SE (2001) Compressive behaviour of softwood under uniaxial loading at different orientations to the grain. Mech Mater 33(12):705-715. https://doi.org/10.1016/S0167-6636(01)00086-2.

Reiterer A, Stanzl-Tschegg SE, Tschegg EK (2000) Mode I fracture and acoustic emission of softwood and hardwood. Wood Sci Tech 34(5):417-430. https://doi.org/10.1007/s002260000056.

Rescalvo FJ, Morillas L, Valverde-Palacios I, Gallego A (2020) Acoustic emission in I-214 poplar wood under compressive loading. Eur J Wood Prod 78(4):723-732. https://doi.org/10.1007/s00107-020-01536-7.

Ritschel F, Brunner AJ, Niemz P (2013) Nondestructive evaluation of damage accumulation in tensile test specimens made from solid wood and layered wood materials. Compos Struct 95(January 2013):44-52. https://doi.org/10.1016/j.compstruct.2012.06.020.

Sato K, Fushitani M, Noguchi M (1984a) Discussion of tensile fracture of wood using acoustic emissions. Estimation of tensile strength and consideration of AE generation based on fracture mechanics. Mokuzai Gakkaishi. J Japan Wood Res Soc 30(2):117-123. https://www.jwrs.org/english/journals/mkz-toce/mkze-30/. (30 August 2024).

Sato K, Kamei N, Fushitani M, Noguchi M (1984b) Discussion of tensile fracture of wood using acoustic emissions: A statistical analysis of the relationships between the characteristics of AE and fracture stress. J Japan Wood Res Soc 30(8):653-659. https://www.jwrs.org/english/journals/mkz-toce/mkze-30/. (30 August 2024).

Sharma K (2017) Investigation of failure in different materials using acoustic emission technique. ME thesis, Thapar University, Patiala, India. 89 pp. https://tudr.thapar.edu:8443/jspui/bitstream/10266/4845/5/4845.pdf. (30 August 2024).

Smardzewski J, Gozdecki C (2007) Decohesion of glue bond in wood connections. Holzfor 61(3):291-293. https://doi.org/10.1515/HF.2007.061.

Southern Forest Products Association (SFPA (2018) Southern pine use guide: Strength, treatability, and beauty. 2018 Edition. Metairie, LA. https://www.southernpine.com/wp-content/uploads/2023/09/SP_USEguide_METRIC_10-18L.pdf. (30 August 2024).

Turkot CG (2019) Preliminary characterization of physical and mechanical properties of species used in staircase manufactures. MS thesis, Mississippi State University, Mississippi State, MS. 45 pp. https://scholarsjunction.msstate.edu/td/3619. (30 August 2024).

Turkot CG, Seale RD, Entsminger ED, França FJN, Shmulsky R (2020) Nondestructive evaluation of red oak and white oak species. Forest Prod J 70(3):370-377. https://doi.org/10.13073/FPJ-D-20-00015.